iScience

CellPress
OPEN ACCESS

Article

A soft crawling robot with a modular design based on electrohydraulic actuator

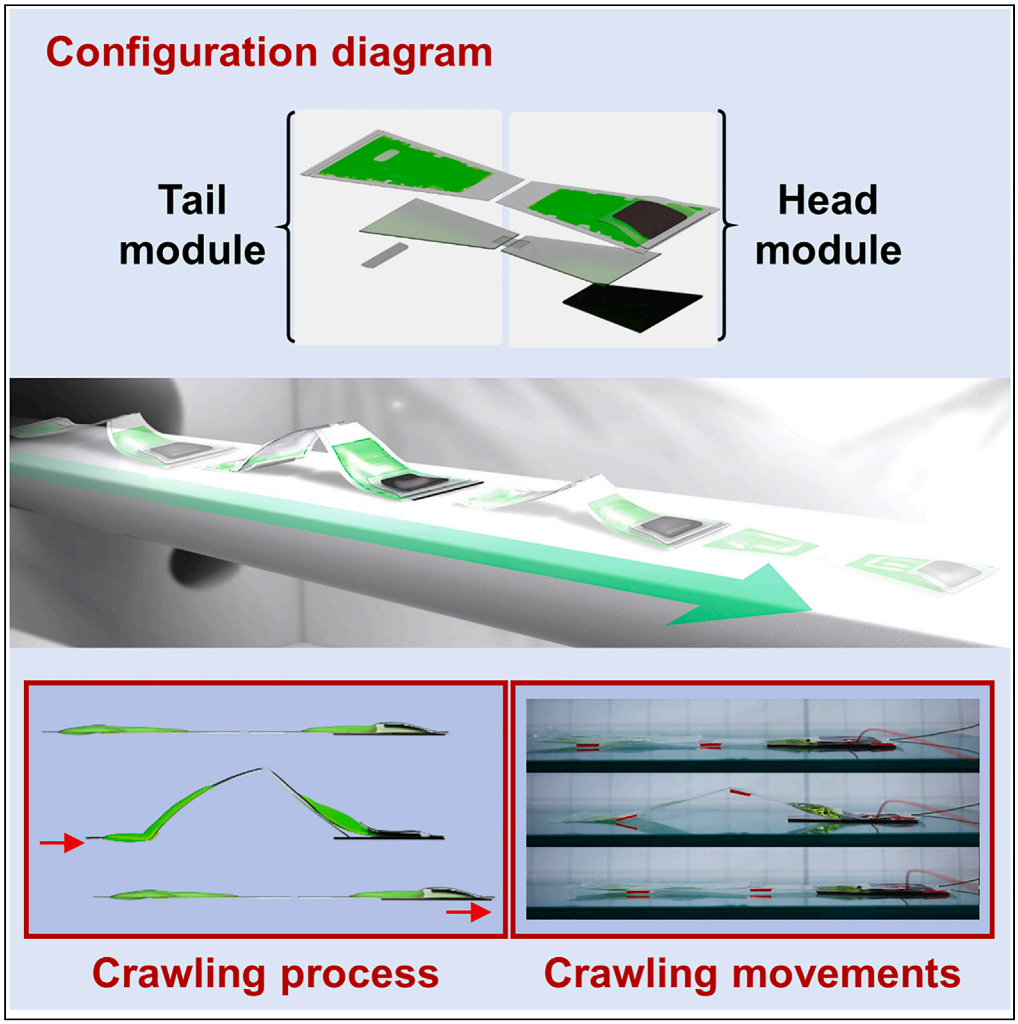

Sohyun Kim,
Youngsu Cha

ys02@korea.ac.kr

Highlights

The soft crawling robot comprised soft modules, a body frame, and contact pads

The soft modules utilized electrostatic and hydraulic forces

The modular robotic design created a deformation similar to peristaltic crawling

The robot carried out forward movement to traverse slopes and narrow crevices

Kim & Cha, iScience 26, 106726
May 19, 2023
https://doi.org/10.1016/j.isci.2023.106726

iScience

CellPress
OPEN ACCESS

Article

A soft crawling robot with a modular design based on electrohydraulic actuator

Sohyun Kim[1] and Youngsu Cha[1,2,*]

SUMMARY

The soft structure of creatures without a rigid internal skeleton can easily adapt to any atypical environment. In the same context, robots with soft structures can change their shape to adapt to complex and varied surroundings. In this study, we introduce a caterpillar-inspired soft crawling robot with a fully soft body. The proposed crawling robot consists of soft modules based on an electrohydraulic actuator, a body frame, and contact pads. The modular robotic design produces deformations similar to the peristaltic crawling behavior of caterpillars. In this approach, the deformable body replicates the mechanism of the anchor movement of a caterpillar by sequentially varying the friction between the robot contact pads and the ground. The robot carries out forward movement by repeating the operation pattern. The robot has also been demonstrated to traverse slopes and narrow crevices.

INTRODUCTION

The migration methods of organisms have evolved to secure efficiency and stability to survive in the natural environment for a long time. Peristaltic movement is considered one of the most effective methods for overcoming unstructured terrain.[1–3] For example, caterpillars can climb tree branches or navigate complex land. They perform gait by sequentially contracting segments and bending them into an omega (Ω) shape.[4–6] Such motion is beneficial for certain movements such as twisting the body or going through narrow gaps. Moreover, caterpillars have a completely soft body without rigid components, which allows them to interact and adapt to changing environments.[7–10] Their adaptability and biologically simple structure have received considerable attention as sources of inspiration for robotic research. The field of robotics has begun to apply the principles of natural models to the exploration and reconnaissance of terrain that is difficult for humans to access. Moreover, it has led to the development of biomimetic and bioinspired robots.

Various types of robots with crawling capabilities have been developed to satisfy the operating and movement requirements within constrained environments.[11–16] One such robot was designed as a peristaltic crawling robot mimicking the movement mechanism of an earthworm; such robots are used for terrestrial exploration and endoscopy.[17–20] They are much more useful for operation and control in narrow spaces compared to multi-legged robots; however, their rigid mechanical components, such as motors and linkages, complicate their structure.

An ongoing challenge in robotics is the design of robots that can adapt to unpredictable environments. Applying softness to robotic design is an attractive solution to this problem because soft robots can change their shape to accommodate complex surroundings.[21,22] The soft structure of animals allows them to interact and adapt to uncertain environments.[23–26] Soft robots offer significant advantages over rigid ones because they use natural soft materials that are safe to operate and easily adapt to the environment.[27] Many soft robots that utilize flexible structures and smart materials have been proposed. Origami-inspired structures incorporating actuators are suitable for creating mechanisms that mimic the movements of soft animals.[28–30] The actuator of the bow structure performs a crawling or rolling motion through bending deformation.[31] Actuators with these geometric designs require special substrates to assist in movement. In addition, robots capable of peristaltic gait using a variety of materials, including soft pneumatic actuators, soft photo actuators, ionic polymer-metal composites (IPMCs), shape memory alloys (SMAs), and dielectric elastomer actuators (DEAs) have been presented. Soft pneumatic actuators have been effectively applied to achieve a peristaltic crawling robot with friction control.[32] However, they always require an external fluid source and must be connected to bulky pumps and valves, limiting their portability.

[1]School of Electrical Engineering, Korea University, Seoul 02841, Republic of Korea

[2]Lead contact

*Correspondence: ys02@korea.ac.kr

https://doi.org/10.1016/j.isci.2023.106726

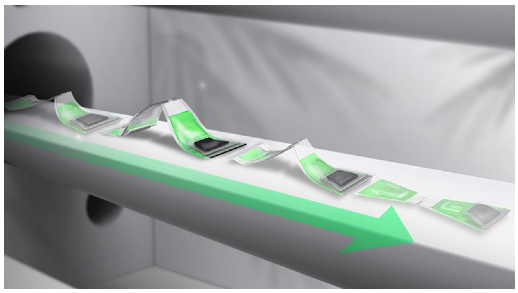

Figure 1. Concept of movement of soft crawling robot

Soft photo actuators generate self-movement without artificial energy and control in response to changes in light intensity.[33,34] Their performances are depending on the brightness factor of the external environment. IPMCs are applied in the development of annular robots owing to their advantages of low weight and high deformation.[35] However, they are not suitable for dry environments because of the limitations of the material under wet conditions. The SMA spring actuators act as a contraction and extension of the earthworm muscle and exhibit a motion similar to that of a real earthworm.[36–40] However, the SMA spring wire limits the speed of movement of the robot, because it takes a relatively long time to recover to its initial state. The SMA coil actuators are installed in the soft body to mimic the behavior of a caterpillar capable of rolling motion.[41] SMA coil actuators are convenient muscle-type actuators but have poor fatigue characteristics.[42] DEAs are promising candidates for application in robots such as annelid because DEA has high energy density, electromechanical efficiency, and fast response speed.[43,44] Dielectric breakdown may occur because of high electric fields. They also require a rigid frame and pre-stretch to work effectively.

Recent innovations have made it possible to overcome the limitations of conventional actuators and enabled the development of flexible electronic devices using electrostatic and hydraulic forces based on hydraulically amplified self-healing electrostatic (HASEL) actuators.[45–47] These actuators have the advantages of both electrostatic and hydraulic actuators by electrostatically changing the distribution of the internal liquid with large strains.[48] They do not require an external source of compressed fluid or pumps. They are easy to control because of the usage of electrical power. In addition, they have excellent deformation without a rigid frame and pre-stretching. We have previously reported that these actuators produce unidirectional and bidirectional bending, rotary, and twisting motions depending on the various module designs.[49–51] Bending and rotational movements are developed using manipulators, such as grippers, and active plates, respectively. In addition, the generated linear motion is applied to a robot capable of forwarding traverse from other research groups.[52] The stacked structure of donut-shaped HASEL actuators allows forward motion, but it remains challenging to pass through narrow gaps because it is difficult to create a wavy curved structure. Thus, it is necessary to modify the various motions and module designs developed thus far to be similar to biological motions. In this study, we introduce a modular soft crawling robot inspired by a caterpillar peristaltic moving mechanism based on bending motion and design by integrating these technologies. Figure 1 shows the conceptual design of the proposed crawling robot.

The proposed soft crawling robot consists of modules based on an electrohydraulic actuator, a body frame, and contact pads. The module is composed of flexible films and a dielectric fluid. In addition, each module is divided into a head module with electrodes and a tail module without electrodes. The two modules are connected using a soft-body frame. This design produces deformations similar to the peristaltic crawling behavior of caterpillars. Forward movement is performed through the cooperation of the two modules. Moreover, the robot can traverse slopes and narrow crevices.

Consequently, these modular soft crawling robots based on electrohydraulic actuators have potential for a wide range of applications, including bioinspired robotics, environmental monitoring, and animal behavior studies. In addition, crawling robots enable unstructured area exploration and small-goods delivery operations.

RESULTS

Bioinspiration design of soft crawling robot

Creatures such as caterpillars have fewer restrictions on shape and form, allowing them to transform with a great degree of freedom. They crawl by contracting their bodies into a wavy shape. Mimicking this

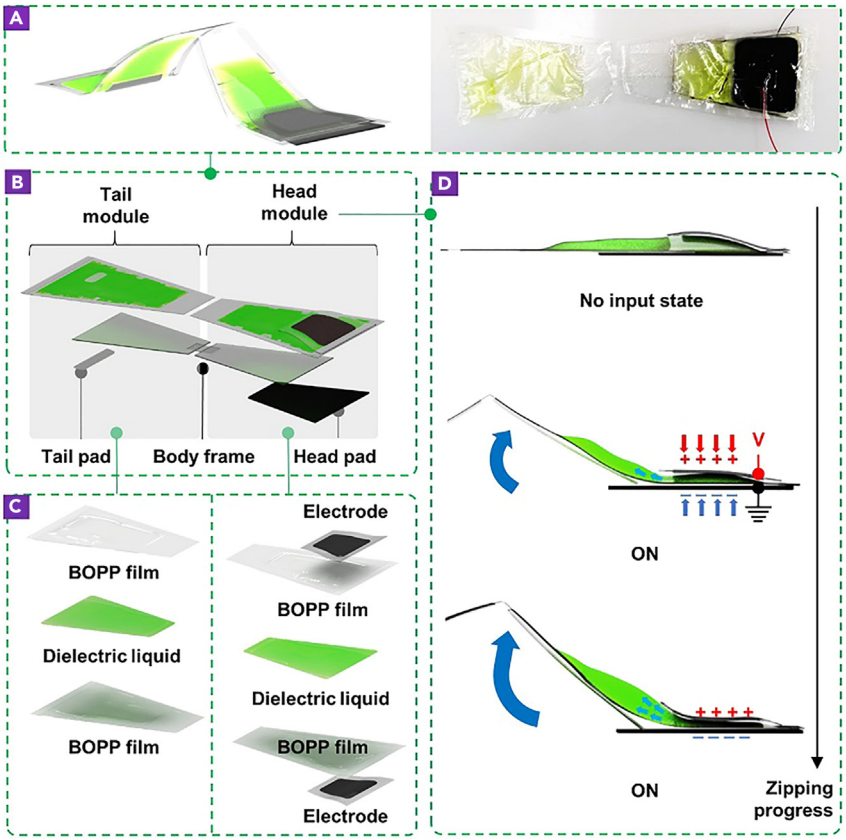

Figure 2. Detailed design of soft crawling robot and operation principle of head module actuator

(A) Schematic and picture of crawling robot.

(B) Configuration diagram for robot fabrication.

(C) Fabrication methods of the head module and tail module.

(D) Operation mechanism of head module actuator.

biological movement using traditional robotic systems is challenging and usually requires complex mechanisms and a large number of actuators. As a novel approach for crawling, we have designed a soft robot with reference to the soft structure of caterpillars. The soft crawling robot is inspired by the body geometry and movement of caterpillars. Figure 2A shows the design and a photograph of the soft crawling robot.

We present a crawling robot with fluid-filled modules similar to a real caterpillar. The robot consists of two modules with a constant volume (head and tail modules), a flexible body frame, and two pads (head and tail pads), as shown in Figure 2B. The two modules are arranged in series and are capable of retracting motion in a wavy shape. The body frame acts as a soft body and makes a natural transition between the retraction and expansion phases in the longitudinal direction. In addition, two pads are attached to the bottom of each module to act as the feet of the robot.

Another approach for making robots adaptable to various environments is to exploit the mechanisms used by organisms in similar environments. The basic mechanism of most peristaltic crawling is friction. Like the feet of the caterpillar, the head and tail pads of the proposed crawling robot play an important role in their movement by acting as a source of friction. When the robot is retracted, it is designed to create high friction with only the head pad abutting the ground and the tail pad not abutting the ground. However, when the robot is stretched in a stable state, the tail pad with relatively high friction is fixed to the ground and the head pad slides off the surface.

Fabrication of soft crawling robot

The soft crawling robot has a caterpillar-inspired design, including head and tail modules. First, the head module as an actuator consists of a shell containing a fluid, wiring materials, and flexible electrodes

(Figure 2C). The module is composed of flexible biaxially oriented polypropylene (BOPP) films and filled with a dielectric liquid. Carbon conductive tape is attached to both sides of the shell surface as a flexible electrode. The tail module is fabricated by a process similar to that used for the head module. Unlike the active head module, the passive tail module does not require electrodes.

The two modules are then attached in series to the body frame to mimic the wavy shape of a caterpillar. A flexible polyethylene terephthalate (PET) film is used as the body frame. The body frame produces a deformation similar to the peristaltic crawling motion of the caterpillar by converting the bending motion of the electrohydraulic actuator into a wavy motion.

Finally, the pads in contact with the ground are fabricated using two materials with different coefficients of friction. The head pad is made by laser-cutting a polyvinyl chloride (PVC) sheet. The head pad is attached to the end of the head module. The flexible tail pad made of silicone rubber exhibits flexibility and high friction. A tail pad is attached to the end of the tail module. Additional fabrication details are provided in the STAR Methods.

Operation mechanism of head module actuator

The completed head module actuator is operated using electrostatic and hydraulic forces as shown in Figure 2D. The head module consists of a flexible but inextensible polymer shell, the interior of which is filled with a dielectric fluid. When the voltage input is "OFF," the actuator is in the resting state. When voltage is applied to the electrodes attached to both sides of the shell, the electrostatic force attracts the electrodes and squeezes the liquid. The fluid is then pushed into a section that is unaffected by the voltage input. Increasing the voltage above a certain value causes a pull-in phenomenon in which the electrode is fully pulled beyond the increase in mechanical restoring force.[45] After pull-in switching, the operating strain of the actuator is further increased. Therefore, as the process progress, the cross-section of the part where the fluid moves become convex. Owing to the non-extensibility of the shell and the pressure of the fluid, the thickness of the cross-section of the non-electrode part is increased and the length of the side is reduced. At the same time, the actuator module demonstrates an upward bending motion owing to the difference in stiffness between the head module and the PET film attached to the bottom of the head module. Changes in the shell cross-section cause bending deformation of the head module, followed by wavy transitions and overall linear contraction of the soft crawling robot.

Operation mechanism of crawling motion

In general, the peristaltic gait of caterpillar crawl is based on an anchor movement mechanism. The movement immobilizes the forepaw and uses the muscles of the middle part to contract the rest of the body. Caterpillars move forward while stretching their front paw with their hind paw fixed. This pattern is repeated to allow caterpillars to crawl along the ground.

As shown in Figure 3A, the crawling motion of the robot involves three steps. (1) If power is not supplied to the head module actuator, it is in its initial state. (2) The head module actuator is operated with a head pad that is firmly fixed to the surface. When the head module actuator operates, it is fixed by its own weight and the head pad is supported from the ground. The bending deformation of the head module pulls the tail module that is connected to the body frame. In this way, the tail pad does not come into contact with the ground, and in the next step, it does come into contact with the ground, causing a high friction value. (3) A robot with a deformable body has wave like deformation and longitudinal movement. The tail pad is supported on the surface when the robot body is bent in a wavy shape by the weight of the tail module. The rear friction is greater than the front friction force owing to the relatively high friction coefficient of silicone. When the head module actuator is turned off, the electrostatic attraction gradually dissipates. The head pad slides off the surface as owing to the restoring force generated by the fluid flow. The body moves forward through stretching. Therefore, the soft crawling robot achieves crawling motion as the head and tail pads are sequentially used as anchors.

With the periodic operation of the head module actuator, the head and tail pads are alternately fixed and driven, and the entire soft robot is moved. One cycle is defined by the inclusion of all three steps of the crawling motion. Stride length is the total distance traveled (X) in one cycle.

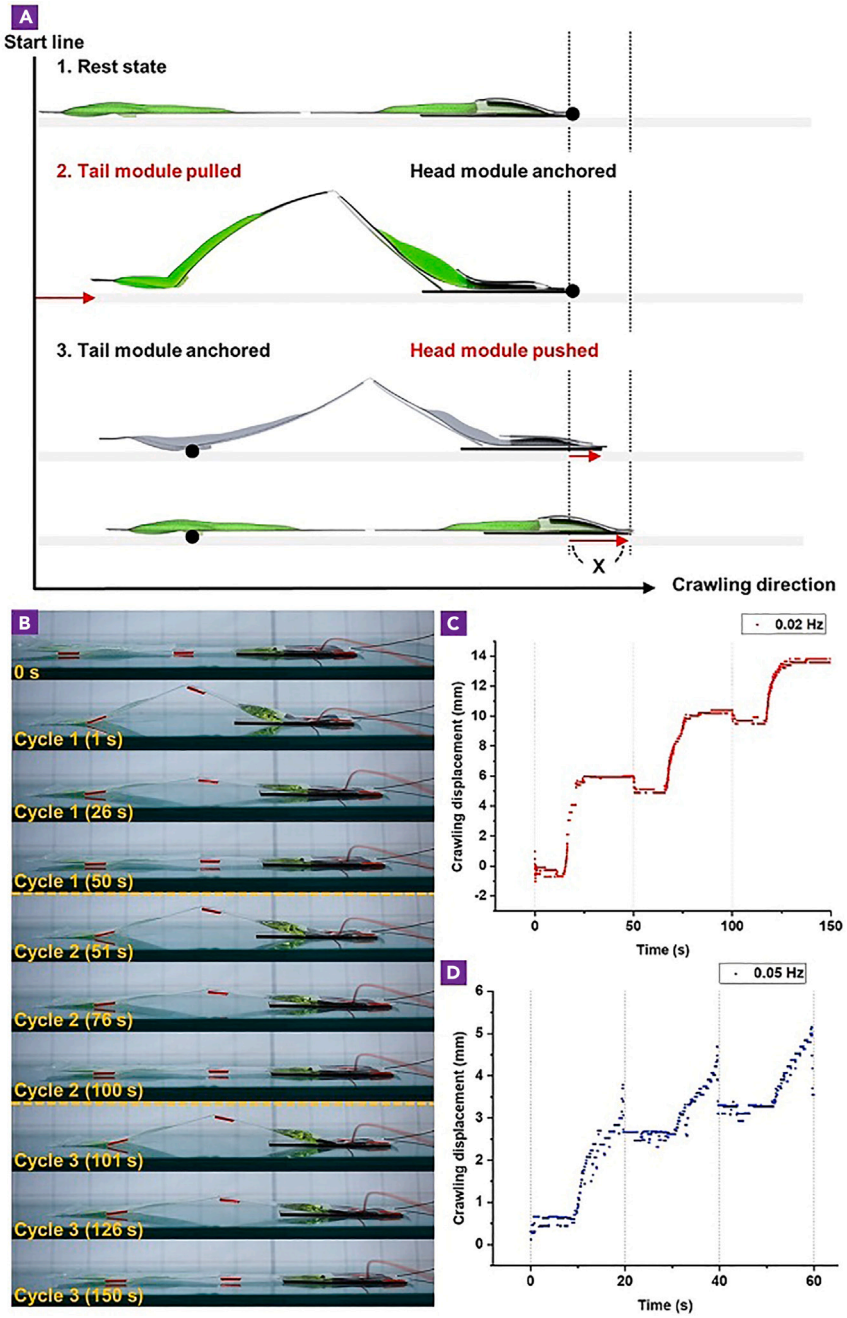

Figure 3. Motion principle and continuous crawling results

(A) Cross-sectional view of crawling process.

(B) Snapshots of soft crawling robot movements on a glass plate.

(C) Crawling displacement result at 0.02 Hz.

(D) Crawling displacement result at 0.05 Hz.

Continuous crawling motion

The anchor movement mechanism allows the soft crawling robot to move in the forward direction. To investigate the operating capability of the crawling robot, movement according to the operating cycle at an input peak-to- peak voltage of 10 kV was investigated. The operating frequency was 0.02 Hz and the square wave had a 20% duty cycle. A detailed description of the circuit configuration and setup for testing is provided in the STAR Methods.

Figure 3B shows the movement according to the sequence of operations of the soft crawling robot on a glass surface. The operating cycle was repeated three times, starting at 0 s. At 0 s, it was the initial state of the robot. At 1 s, when an input voltage was applied to the head module actuator, the shell cross-section of the head module became preferentially convex. This deformation caused a bending deformation of the robot body. When the head pad was fixed, the tail module and tail pad were pulled forward. Therefore, longitudinal contraction of the robot occurred. The tail pad, which has a relatively high friction force, remained fixed to the surface. After supplying voltage for 10 s, the electrostatic attraction of the head module gradually disappeared. Then, the head pad slid as the fluid in the head module returned to its initial state. At 26 s, the robot was shown in a state of being stretched forward. At 50 s, the robot reached its initial resting state. The soft crawling robot therefore realized crawling motion with repeated movements in sequence. A video demonstrating the crawling behavior of the robot is shown in Video S1.

The operational performance of the soft robot was tested for the input frequency of the head module actuator. Optical data were acquired using a motion-tracking program. A detailed description of the recording and motion tracking is provided in the STAR Methods.

The crawling distance traveled by the robot over a certain period is shown in Figure 3C. The input signal was a square wave with an input voltage of 10 kV, operating frequency of 0.02 Hz, and a 20% duty cycle. The stride length moved at the tip of the head module was measured over three cycles. In the first cycle, the head module started moving 4.06 s after the applied voltage was turned off. The robot body moved forward while stretching for 11.04 s. The soft crawling robot was considered to have reached a steady state from the second operating cycle onwards. It can be seen that the robot was gradually pushed forward after the voltage was turned off and 6.45 s later. It took approximately 11.76 s for the robot body to fully unfold. The peak-to-peak displacements for cycles 1, 2, and 3 were approximately 6.96, 5.51, and 4.31 mm, respectively.

Next, we changed the input signal frequency of the head module actuator to 0.05 Hz under the same amplitude condition. The input signal was a square wave with a 20% duty cycle. The crawling distance of the robot in the time domain is shown in Figure 3D. In the first cycle, the applied voltage was turned off and after 5.30 s the crawling robot started to move. It was stretched almost immediately for 10.70 s. In the steady state, the voltage was turned off, started moving after 6.97 s and returned to its initial space after approximately 9.04 s. This value is the average of the second and third cycles. The peak-to-peak displacements for cycles 1, 2, and 3 were approximately 3.67, 2.38, and 2.22 mm, respectively.

The results showed that it took a certain amount of time for the voltage applied to the head module to turn off and for the charge to be completely discharged. In addition, the robot required a recovery time of approximately 9–11 s to fully unfold as it slipped. This probably indicates that higher operating frequencies may not have sufficient release time for liquid movement.[50] It was determined that a low operating frequency was more conducive to the operation of the robot.

Mathematical modeling of soft crawling robot

A mathematical model of the robot was developed for the proposed crawling robot. A theoretical understanding of the design provides a means of predicting the movements of robots without conducting actual tests. Figure 4A shows the modeling schematic of the soft robot.

Given the properties of the soft crawling robot, it has been modeled as a system consisting of a massless spring, a damper, and two masses in the horizontal plane.[53] The generally known force equilibrium equations for the two masses can be established as

$$\begin{aligned} m_T\ddot{x}_T(t) + m_H x_T(t) + c\dot{x}_T(t) - kx_H(t) - c\dot{x}_H(t) &= -f_T(t) \\ m_H\ddot{x}_H(t) - kx_T(t) - c\dot{x}_T(t) + kx_H(t) + c\dot{x}_H(t) &= F(t) - f_H(t), \end{aligned} \quad \text{(Equation 1)}$$

where m_H , m_T , k, c, F , f_H , and f_T are the masses of the head and tail modules, spring constant, damping coefficient, driving force for operation of the robot, and frictional forces generated by the head and tail modules, respectively. t is the time variable. In addition, x_H and x_T as the end positions of m_H and m_T, respectively.

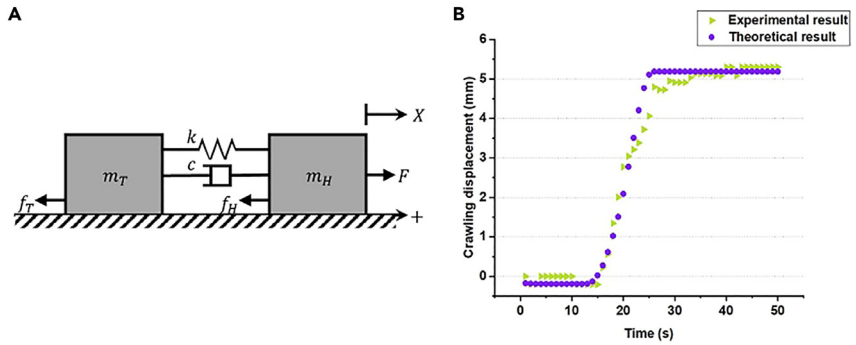

Figure 4. Mathematical model of soft crawling robot and modeling results

(A) Double mass-spring-damper model of robot.

(B) Comparison of experimental and theoretical results.

When both paws of the caterpillar are actuated simultaneously, an equal amount of force is created on the walking surface, preventing the caterpillar from moving in either direction. Anisotropic friction is required at one end to convert the caterpillar bending motion into a forward motion. Based on this, the robot model alternately applies friction forces according to its relative motion with respect to the surface. The friction force associated with each pad can be expressed according to the established method[54] as

$$f_i(t) = \begin{Bmatrix} \text{sign}[\dot{x}_i(t)]\mu_i m_i g & \text{if } |\dot{x}_i(t)| \geq v_i \\ 0 & \text{if } |\dot{x}_i(t)| < v_i \end{Bmatrix}, \quad i = T(Tail) \text{ or } H(Head), \qquad \text{(Equation 2)}$$

where μ_i and g are the friction coefficient and the gravitational acceleration constant, respectively. In addition, v_i is the transition boundary condition for anisotropic friction. v_i is defined in a narrow range close to zero. When the mass starts to slide and the velocity satisfies the boundary condition, it is affected by friction. When the velocity does not satisfy this condition, the friction force is assumed to be zero.

The electrostatic force generated by the voltage causes the dielectric liquid to flow to the non-electrode part and generates kinetic energy. When the voltage is released, the stored energy returns the dielectric liquid to its initial state and provides energy for the soft crawling robot to move forward. After all, the driving force for the forward motion of the crawling robot is derived from the electrostatic force applied to the head module actuator. It is assumed that the driving force and input voltage of the head module actuator share the same frequency of 0.02 Hz and the same 20% duty cycle. As shown in Figure 3C, the crawling robot starts moving approximately 17 s after a voltage is applied to the head module actuator in a steady state. Therefore, the driving force is set to have a time delay of 17 s compared to the input voltage signal. The driving force is derived from a Fourier series representation.[55] Specifically, a periodic even-pulse function of a cosine series is considered. This function has an amplitude α, a period of 50 s, and a pulse width of 10 s. The electrically induced driving force applied to the robot can be approximated as follows, as

$$F(t) = \alpha\left(0.2 + 0.3744\cos\left(\frac{1}{8}(t-17)\right) + 0.3029\cos\left(\frac{2}{8}(t-17)\right) + 0.0936\cos\left(\frac{4}{8}(t-17)\right) - 0.0624\cos\left(\frac{6}{8}(t-17)\right) - 0.0865\cos\left(\frac{7}{8}(t-17)\right)\right), \qquad \text{(Equation 3)}$$

where α is a constant that adjusts the magnitude of the force.

The modeling results have been solved numerically using 'NDSolve' in MATHEMATICA. The parameters are summarized in Table 1. The values of k, c, and α have been manually fitted using the experimental results shown in Figure 3C. The masses have been measured using a scale. The friction coefficient of the head pad has been measured using a friction coefficient measuring equipment. The friction coefficient of the tail pad has been cited.[56]

Figure 4B shows the stride length X (= $x_H(t)$) of the crawling robot during steady state motion. The X data points are shifted to the origin. The predicted deformation of the crawling robot is first fixed before moving forward, and then slowly moves forward in the direction of travel. This movement pattern is similar to the

Table 1. Parameters for the equations

Parameter	Value
k	10^{-5} N/m
c	10^{-1} N/m
α	0.37
m_T	2 g
m_H	6 g
μ_T	0.61
μ_H	0.22
g	9.81 m/s^2

anchor mechanism of the forelimbs observed in the caterpillar gait. The theoretical results are consistent with the reformation observed in the experiment. The R^2 value is 0.9809. Although there is a small discrepancy, our model can provide a mean of analyzing the performance of the robot.

The electrical energy generated by the head module actuator is converted into kinetic energy for forward crawling of the soft crawling robot. Because the magnitude of the electric field rapidly decreases in the non-electrode part of the head module actuator, only the electrical energy stored in the electrode part is considered.[57,58] Assuming that there is no liquid between the compression films after fully adhesion, the compressed region is treated as a parallel plate capacitor.[59] The electrical energy E_e stored in the electric field between the electrodes is expressed as

$$E_e = \frac{1}{2}CV^2 = \frac{1}{2}\left(\varepsilon_r\varepsilon_0\frac{A}{d}\right)V^2, \quad \text{(Equation 4)}$$

where C is the dielectric fluid capacitance, V is the input voltage, ε_r is the relatively permittivity of dielectric fluid, ε_0 is the dielectric constant in vacuum, A is the size of the electrode, and d is the distance between the electrodes. The parameters used in the equation are summarized in Table 2. Electrical energy was calculated to be approximately 27.8 mJ. Although the soft crawling robot moves forward from its initial stop state, the kinetic energy E_k can be equated to the work done W by the driving force by the work-kinetic energy theorem.

$$E_k = W = F\Delta x, \quad \text{(Equation 5)}$$

where F is the magnitude of the driving force, and Δx is the stride length change of the crawling robot. The driving force applied while the crawling robot moves forward is calculated as a constant value through Equation 3. The parameters used in the equation are summarized in Table 2. Kinetic energy was calculated to be approximately 2.117 10^{-5} mJ. Therefore, the electrical energy stored in the head module actuator is converted into energy required for the pressure energy of the dielectric liquid and geometric deformation. Some of the energy is lost as thermal energy generated by frictional forces. The efficiency of the energy converted to the working deformation in the crawling robot becomes lower.

Demonstration at other conditions

Experiments were conducted to further demonstrate the ability of the soft crawling robot to move in a confined environment. The robot was operated with the same input signal as that in the continuous

Table 2. Parameters for the equations

Parameter	Value
ε_r	3.2
ε_0	$8.854 \cdot 10^{-12}$ F/m
A	0.0011 m^2
d	0.000056 m
V	10 kV
F	$0.3041 \cdot 10^{-5}$ N
Δx	$6.960 \cdot 10^{-3}$ m

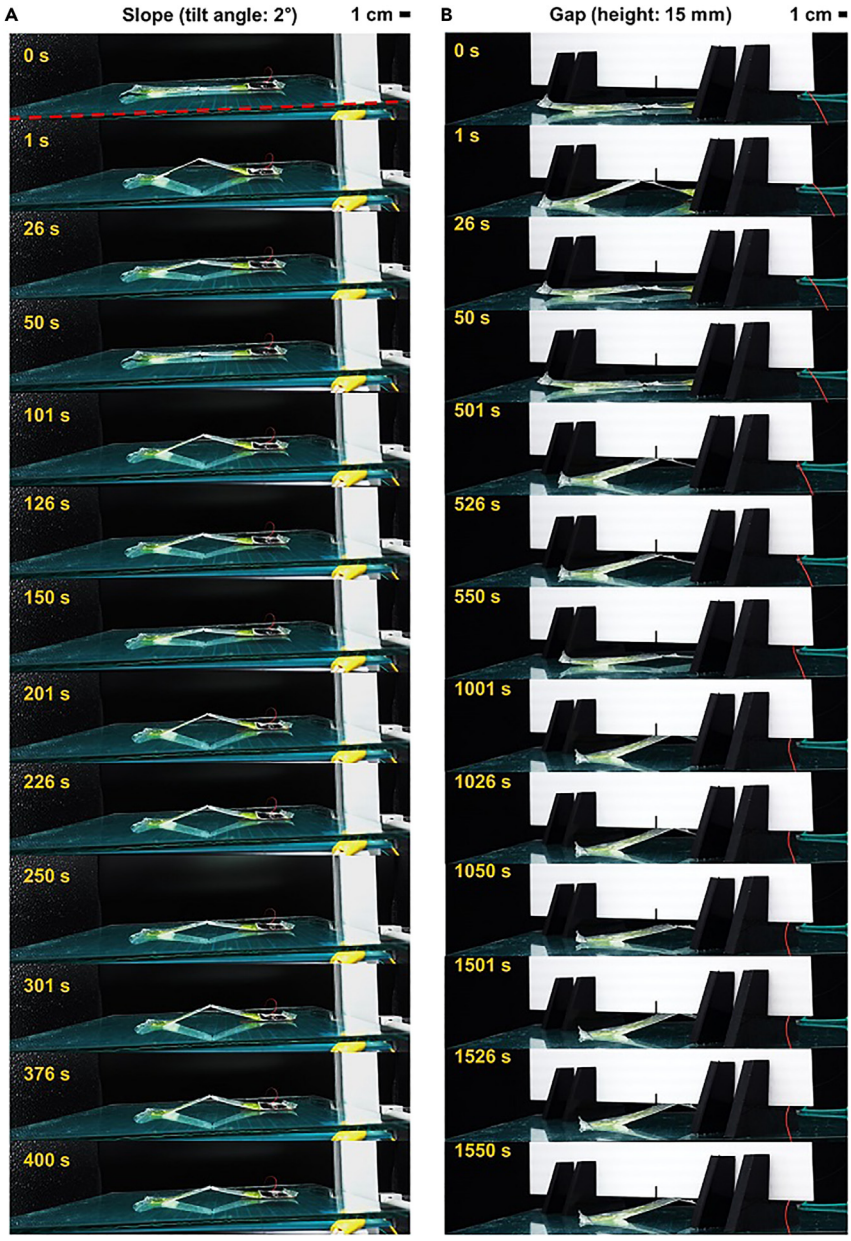

Figure 5. Demonstration results of soft crawling robot

(A) Snapshots of climbing slope test.

(B) Snapshots of test regarding passing through the narrow gap.

crawling motion experiment. A voltage of 10 kV and an operating frequency of 0.02 Hz were applied. Figure 5 shows the images of the crawling robot at each time step.

Figure 5A shows the soft crawling robot climbing a glass plate with an inclination angle of 2° to the ground. A crawling robot on an incline took more time than horizontal movement because it was prone to sliding in the opposite direction under its weight. A video of the robot climbing a slope is provided in Video S2.

Figure 5B displays the soft crawling robot passing through a crevice. The gap was made up of an acrylic plate at a height of 15 mm from the ground. The crawling robot crawled into the crevice by alternately

Table 3. Comparison with other soft crawling robots

Soft crawling robot	Actuator type	Thickness (mm)	Mass (g)	Linear speed (mm/s)	Body length (mm)
Proposed one	Electrohydraulic	2.5	8	0.1392	125
Zou et al.[63]	Pneumatic	~60	450~810	~5	154
Umedachi et al.[42]	SMA	12	–	112	199
Cao et al.[43]	DEA + Electroadhesion	Body(2) + Feet(–)	–	4.16	208
Mitchell et al.[52]	HASEL	50	~240	14.75	~140

anchoring its pads. When the back of the robot touched the obstacle, the height of its body was limited by the gap. The crawling robot detected the structure and moved forward, unaffected by external factors. This is an advantage for soft robots. The narrow-gap motion proved that the robot has very good environmental adaptability and autonomous movement ability. A video of the robot going through this gap is shown in Video S3.

DISCUSSION

In this study, a caterpillar-inspired soft crawling robot is presented. The main advantage of using electrohydraulic materials as a design method for mimicking wavy gait is low weight and high deflection. Typical HASEL crawling actuators did not use wavy shape bending.[52] We have provided new possibilities for the crawling method by combining modules based on an electrohydraulic actuator, a body frame, and contact pads. The modular design results in movement variations similar to the peristaltic crawling behavior of caterpillars. The modular structure of the robot can be easily extended, which demonstrates the potential to create robots of various lengths. Directional control can be achieved using a parallel combination of modules. This is a further research area inspired in part by other concepts and ideas.[60,61] The developed soft robot has the ability to pass through obstacles in a confined space owing to its thin thickness and the total weight of 8 g. Table 3 shows the specification comparison data of our crawling robot and conventional crawling robots made by soft actuators. Several soft crawling robots have achieved high speed performance at the expense of design parameters such as thickness and weight. Fast performance is often an important advantage, but crawling speed alone is not enough to describe all aspects of a system. The thin body is a good alternative for getting through narrow gaps. Lightweight is an indicator for the energy efficiency of soft robots. Moreover, the developed robot is possible to predict the operational performance of the robot by understanding the theoretical model without additional fabrication. A mathematical model may include parameter optimization. The proposed crawling robot has been modeled as a dual-mass spring damper system. The results have been verified by comparison with the experimental data. The prediction of the robot behavior has been modeled empirically because the actuation response was highly non-linear. Other theoretical models can be built for the control and manufacturing optimization of the system. The robot has been experimentally implemented using continuous peristaltic crawling. This demonstration also confirms its applicability to a variety of environments, including slopes and narrow crevices. The motion is generated and controlled along the friction coefficients of the robot pads, whereas the head module actuators periodically provide mechanical power. The non-slip fixed pad improves the movement efficiency of the robot and allows it to crawl over complex terrain. The relatively sufficient surface roughness of the substrate compared to the glass surface used in the experiment prevents the robot from slipping during continuous motion.[62] However, the friction of the pad is difficult to maintain on wet surfaces, so there is little possibility of crawling on wet surfaces.[32] Following this point of view, we look forward to the development of scalable multi-module crawling robots that can adapt to uneven terrain and various surfaces. The operating performance also depends on the input signal. Continuously applying voltages of the same polarity causes charge to be retained and accumulated. This prevents the liquid dielectric from fully returning to its initial position.[62] Reversing the polarity in a continuous cycle relieves charge retention and improves performance.

We have identified the potential for adaptability and autonomous mobility of soft crawling robots. The proposed robotic concept offers new possibilities for soft bioinspired robots. Future research is expected to further explore robotic systems that enable steering and movement on uneven terrains.

Limitations of the study

The operation of the soft crawling robot fabricated and tested in this study has relatively large deviations owing to the handmade process of fabrication. In addition, crawling robots require external wires and

power, which limit their functionality in real-world environments. This problem can be solved by developing robots with embedded systems such as power and control circuits.

The non-linear response of soft crawling robots based on electrohydraulic actuation assumes several conditions for solving mathematical models. A simplified theoretical model can provide insight into the response of soft crawling robots. These insights can be used to guide actuator design. However, some assumptions can make discrepancies in accurately predicting changes in robots. The mathematical model should be studied further to minimize the differences within the real system.

Future research on this topic will focus on attaching lightweight and flexible sensors to crawling robots to detect the external environment. The posture and position of the robot can be adjusted based on sensor information. Soft crawling robots integrated with sensors can be utilized for applications such as animal behavior and transport operation studies.

STAR★METHODS

Detailed methods are provided in the online version of this paper and include the following:

- KEY RESOURCES TABLE
- RESOURCE AVAILABILITY
  - Lead contact
  - Materials availability
  - Data and code availability
- METHOD DETAILS
  - Fabrication details
  - Circuit configuration
  - Recording and motion tracking

SUPPLEMENTAL INFORMATION

Supplemental information can be found online at https://doi.org/10.1016/j.isci.2023.106726.

ACKNOWLEDGMENTS

This work was supported by the National Research Foundation of Korea (NRF) through the Ministry of Science and ICT (MSIT), Korean Government under Grant 2021M3E5D2A01023887.

The authors would like to thank Mr.Gyung Min Lee for the help with drawing schematic.

AUTHOR CONTRIBUTIONS

S. K. designed research, performed research, analyzed data, and wrote the paper; and Y.C. supervised the experimental analysis.

DECLARATION OF INTERESTS

The authors declare that they have no known competing financial interests or personal relationships that could have appeared to influence the work reported in this paper.

INCLUSION AND DIVERSITY

While citing references scientifically relevant for this work, we also actively worked to promote gender balance in our reference list. We support inclusive, diverse, and equitable conduct of research.

Received: October 11, 2022
Revised: December 26, 2022
Accepted: April 20, 2023
Published: April 26, 2023

REFERENCES

1. Dowling, K.J. (1997). Limbless Locomotion: Learning to Crawl with a Snake Robot (Carnegie Mellon University).
2. Gans, C. (1975). Tetrapod limblessness: evolution and functional corollaries. Am. Zool. *15*, 455–467.
3. Simon, M.A., Woods, W.A., Jr., Serebrenik, Y.V., Simon, S.M., van Griethuijsen, L.I., Socha, J.J., Lee, W.K., and Trimmer, B.A. (2010). Visceral-locomotory pistoning in crawling caterpillars. Curr. Biol. *20*, 1458–1463.
4. Quillin, K.J. (1999). Kinematic scaling of locomotion by hydrostatic animals: ontogeny of peristaltic crawling by the earthworm lumbricus terrestris. J. Exp. Biol. *202*, 661–674.
5. van Griethuijsen, L.I., and Trimmer, B.A. (2014). Locomotion in caterpillars. Biol. Rev. *89*, 656–670.
6. Wang, W., Wang, Y., Wang, K., Zhang, H., and Zhang, J. (2008). Analysis of the kinematics of module climbing caterpillar robots. In IEEE/ASME International Conference on Advanced Intelligent Mechatronics (IEEE), pp. 84–89.
7. Chen, S., Cao, Y., Sarparast, M., Yuan, H., Dong, L., Tan, X., and Cao, C. (2020). Soft crawling robots: design, actuation, and locomotion. Adv. Mater. Technol. *5*, 1900837.
8. Gu, G., Zou, J., Zhao, R., Zhao, X., and Zhu, X. (2018). Soft wall-climbing robots. Sci. Robot. *3*, eaat2874.
9. Saga, N., and Nakamura, T. (2004). Development of a peristaltic crawling robot using magnetic fluid on the basis of the locomotion mechanism of the earthworm. Smart Mater. Struct. *13*, 566–569.
10. Trimmer, B.A., and Lin, H.t. (2014). Bone-free: Soft Mechanics for Adaptive Locomotion (Oxford University Press).
11. Chen, J., Wu, J., Luo, M., and Zhang, J. (2014). A knitro-based real-time locomotion method for imitating the caterpillar-like climbing strategy. In 11th IEEE International Conference on Control & Automation (ICCA) (IEEE), pp. 145–150.
12. Chowdhury, A., Ansari, S., and Bhaumik, S. (2017). Earthworm like modular robot using active surface gripping mechanism for peristaltic locomotion. In Proceedings of the Advances in Robotics (Association for Computing Machinery), pp. 1–6.
13. Nakamura, T., and Iwanaga, T. (2008). Locomotion strategy for a peristaltic crawling robot in a 2-dimensional space. In IEEE International Conference on Robotics and Automation (IEEE), pp. 238–243.
14. Song, C.W., Lee, D.J., and Lee, S.Y. (2016). Bioinspired segment robot with earthworm-like plane locomotion. J. Bionic Eng. *13*, 292–302.
15. Tsakiris, D.P., Sfakiotakis, M., Menciassi, A., La Spina, G., and Dario, P. (2005). Polychaete-like undulatory robotic locomotion. In Proceedings of the 2005 IEEE International Conference on Robotics and Automation (IEEE), pp. 3018–3023.
16. Wang, K., Yan, G., Jiang, P., and Ye, D. (2008). A wireless robotic endoscope for gastrointestine. IEEE Trans. Robot. *24*, 206–210.
17. Omori, H., Hayakawa, T., and Nakamura, T. (2008). Locomotion and turning patterns of a peristaltic crawling earthworm robot composed of flexible units. In IEEE/RSJ International Conference on Intelligent Robots and Systems (IEEE), pp. 1630–1635.
18. Omori, H., Nakamura, T., Iwanaga, T., and Hayakawa, T. (2010). Development of mobile robots based on peristaltic crawling of an earthworm. In Robotics 2010 Current and Future Challenges, pp. 299–319.
19. Wang, K., Yan, G., Ma, G., and Ye, D. (2009). An earthworm-like robotic endoscope system for human intestine: design, analysis, and experiment. Ann. Biomed. Eng. *37*, 210–221.
20. Zuo, J., Yan, G., and Gao, Z. (2005). A micro creeping robot for colonoscopy based on the earthworm. J. Med. Eng. Technol. *29*, 1–7.
21. Hawkes, E.W., Blumenschein, L.H., Greer, J.D., and Okamura, A.M. (2017). A soft robot that navigates its environment through growth. Sci. Robot. *2*, eaan3028.
22. Kovač, M. (2014). The bioinspiration design paradigm: a perspective for soft robotics. Soft Robot. *1*, 28–37.
23. Accoto, D., Castrataro, P., and Dario, P. (2004). Biomechanical analysis of oligochaeta crawling. J. Theor. Biol. *230*, 49–55.
24. Cortez, R., Fauci, L., Cowen, N., and Dillon, R. (2004). Simulation of swimming organisms: coupling internal mechanics with external fluid dynamics. Comput. Sci. Eng. *6*, 38–45.
25. Lin, H.T., and Trimmer, B.A. (2010). The substrate as a skeleton: ground reaction forces from a soft-bodied legged animal. J. Exp. Biol. *213*, 1133–1142.
26. Simon, M.A., and Trimmer, B.A. (2009). Movement encoding by a stretch receptor in the soft-bodied caterpillar, manduca sexta. J. Exp. Biol. *212*, 1021–1031.
27. Tolley, M.T., Shepherd, R.F., Mosadegh, B., Galloway, K.C., Wehner, M., Karpelson, M., Wood, R.J., and Whitesides, G.M. (2014). A Resilient, Untethered Soft Robot (Soft Robot).
28. Fang, H., Zhang, Y., and Wang, K.W. (2017). Origami-based earthworm-like locomotion robots. Bioinspir. Biomim. *12*, 065003.
29. Onal, C.D., Wood, R.J., and Rus, D. (2013). An origami-inspired approach to worm robots. IEEE ASME Trans. Mechatron. *18*, 430–438.
30. Yu, M., Yang, W., Yu, Y., Cheng, X., and Jiao, Z. (2020). A crawling soft robot driven by pneumatic foldable actuators based on miura-ori. Actuators *9*, 26.
31. Liu, Z., Zhang, R., Xiao, Y., Li, J., Chang, W., Qian, D., and Liu, Z. (2021). Somatosensitive film soft crawling robots driven by artificial muscle for load carrying and multi-terrain locomotion. Mater. Horiz. *8*, 1783–1794.
32. Ning, J., Ti, C., and Liu, Y. (2017). Inchworm inspired pneumatic soft robot based on friction hysteresis. Int. J. Robot Autom. *1*, 54–63.
33. Hu, Y., Yang, L., Yan, Q., Ji, Q., Chang, L., Zhang, C., Yan, J., Wang, R., Zhang, L., Wu, G., et al. (2021). Self-locomotive soft actuator based on asymmetric microstructural ti3c2t x mxene film driven by natural sunlight fluctuation. ACS Nano *15*, 5294–5306.
34. Li, J., Zhang, R., Mou, L., Jung de Andrade, M., Hu, X., Yu, K., Sun, J., Jia, T., Dou, Y., Chen, H., et al. (2019). Photothermal bimorph actuators with in-built cooler for light mills, frequency switches, and soft robots. Adv. Funct. Mater. *29*, 1808995.
35. Arena, P., Bonomo, C., Fortuna, L., Frasca, M., and Graziani, S. (2006). Design and control of an ipmc wormlike robot. IEEE Trans. Syst. Man Cybern. B Cybern. *36*, 1044–1052.
36. Chatterjee, S., Niiyama, R., and Kawahara, Y. (2017). Design and development of a soft robotic earthworm with hydrostatic skeleton. In IEEE International Conference on Robotics and Biomimetics (ROBIO) (IEEE), pp. 1–6.
37. Kheirikhah, M.M., Rabiee, S., and Edalat, M.E. (2010). A review of shape memory alloy actuators in robotics. In Robot Soccer World Cup, pp. 206–217.
38. Kim, B., Lee, M.G., Lee, Y.P., Kim, Y., and Lee, G. (2006). An earthworm like micro robot using shape memory alloy actuator. Sens. Actuator A Phys. *125*, 429–437.
39. Kim, M.S., Chu, W.S., Lee, J.H., Kim, Y.M., and Ahn, S.H. (2011). Manufacturing of inchworm robot using shape memory alloy (sma) embedded composite structure. Int. J. Precis. Eng. Manuf. *12*, 565–568.
40. Menciassi, A., Gorini, S., Pernorio, G., Weiting, L., Valvo, F., and Dario, P. (2004). Design, fabrication and performances of a biomimetic robotic earthworm. In IEEE International Conference on Robotics and Biomimetics (IEEE), pp. 274–278.
41. Lin, H.T., Leisk, G.G., and Trimmer, B. (2011). Goqbot: a caterpillar- inspired soft-bodied rolling robot. Bioinspir. Biomim. *6*, 026007.
42. Umedachi, T., Vikas, V., and Trimmer, B.A. (2016). Softworms: the design and control of non-pneumatic, 3d-printed, deformable robots. Bioinspir. Biomim. *11*, 025001.
43. Cao, J., Qin, L., Liu, J., Ren, Q., Foo, C.C., Wang, H., Lee, H.P., and Zhu, J. (2018). Untethered soft robot capable of stable locomotion using soft electrostatic actuators. Extreme Mech. Lett. *21*, 9–16.

44. Li, W.B., Zhang, W.M., Zou, H.X., Peng, Z.K., and Meng, G. (2018). A fast rolling soft robot driven by dielectric elastomer. IEEE ASME Trans. Mechatron. *23*, 1630–1640.

45. Acome, E., Mitchell, S.K., Morrissey, T.G., Emmett, M.B., Benjamin, C., King, M., Radakovitz, M., and Keplinger, C. (2018). Hydraulically amplified self-healing electrostatic actuators with muscle-like performance. Science *359*, 61–65.

46. Kellaris, N., Rothemund, P., Zeng, Y., Mitchell, S.K., Smith, G.M., Jayaram, K., and Keplinger, C. (2021). Spider-inspired electrohydraulic actuators for fast, soft-actuated joints. Adv. Sci. *8*, 2100916.

47. Rothemund, P., Kellaris, N., Mitchell, S.K., Acome, E., and Keplinger, C. (2021). Hasel artificial muscles for a new generation of lifelike robots—recent progress and future opportunities. Adv. Mater. *33*, 2003375.

48. Mitchell, S.K., Wang, X., Acome, E., Martin, T., Ly, K., Kellaris, N., Venkata, V.G., and Keplinger, C. (2019). An easy-to-implement toolkit to create versatile and high-performance hasel actuators for untethered soft robots. Adv. Sci. *6*, 1900178.

49. Kim, S., and Cha, Y. (2020). Rotary motion and manipulation using electrohydraulic actuator with asymmetric electrodes. IEEE Rob. Autom. Lett. *5*, 3945–3951.

50. Kim, S., and Cha, Y. (2022). Electrohydraulic actuator based on multiple pouch modules for bending and twisting. Sens. Actuator A Phys. *337*, 113450.

51. Park, T., Kim, K., Oh, S.R., and Cha, Y. (2020). Electrohydraulic actuator for a soft gripper. Soft Robot. *7*, 68–75.

52. Mitchell, S.K., Martin, T., and Keplinger, C. (2022). A pocket-sized ten channel high voltage power supply for soft electrostatic actuators. Adv. Mater. Technol. *7*, 2101469.

53. Ge, J.Z., Calderón, A.A., Chang, L., and Pérez-Arancibia, N.O. (2019). An earthworm-inspired friction-controlled soft robot capable of bidirectional locomotion. Bioinspir. Biomim. *14*, 036004.

54. Cull, S.J., and Tucker, R.W. (1999). On the modelling of Coulomb friction. J. Phys. Math. Gen. *32*, 2103–2113.

55. Tolstov, G.P. (2012). Fourier Series (Courier Corporation).

56. Champatiray, C., Mahanta, G., Pattanayak, S., and Mahapatra, R. (2020). Analysis for material selection of robot soft finger used for power grasping. In Innovative Product Design and Intelligent Manufacturing Systems (Springer), pp. 961–970.

57. Kellaris, N., Venkata, V.G., Rothemund, P., and Keplinger, C. (2019). An analytical model for the design of peano-hasel actuators with drastically improved performance. Extreme Mech. Lett. *29*, 100449.

58. Moretti, G., Duranti, M., Righi, M., Vertechy, R., and Fontana, M. (2018). Analysis of dielectric fluid transducers. In Electroactive Polymer Actuators and Devices (EAPAD) (SPIE), pp. 142–154.

59. Rothemund, P., Kellaris, N., and Keplinger, C. (2019). How inhomogeneous zipping increases the force output of peano-hasel actuators. Extreme Mech. Lett. *31*, 100542.

60. Lu, X., Wang, K., and Hu, T. (2020). Development of an annelid-like peristaltic crawling soft robot using dielectric elastomer actuators. Bioinspir. Biomim. *15*, 046012.

61. Qin, L., Liang, X., Huang, H., Chui, C.K., Yeow, R.C.H., and Zhu, J. (2019). A versatile soft crawling robot with rapid locomotion. Soft Robot. *6*, 455–467.

62. Chen, R., Yuan, Z., Guo, J., Bai, L., Zhu, X., Liu, F., Pu, H., Xin, L., Peng, Y., Luo, J., et al. (2021). Legless soft robots capable of rapid, continuous, and steered jumping. Nat. Commun. *12*, 7028–7112.

63. Zou, J., Lin, Y., Ji, C., and Yang, H. (2018). A reconfigurable omnidirectional soft robot based on caterpillar locomotion. Soft Robot. *5*, 164–174.

64. Kim, S., and Cha, Y. (2021). Double-layered electrohydraulic actuator for bi- directional bending motion of soft gripper. In 2021 18th International Conference on Ubiquitous Robots (UR) (IEEE), pp. 645–649.

65. Tan, H., Liang, S., Yu, X., Song, X., Huang, W., and Zhang, L. (2019). Controllable kinematics of soft polymer actuators induced by interfacial patterning. J. Mater. Chem. C *7*, 5410–5417.

66. Afolayan, M.O., Yawas, D.S., Folayan, C.O., and Aku, S.Y. (2012). Mechanical description of a hyper-redundant robot joint mechanism used for a design of a biomimetic robotic fish. J. Robot. *2012*, 1–16.

67. Dilibal, S., Sahin, H., and Celik, Y. (2018). Experimental and numerical analysis on the bending response of the geometrically gradient soft robotics actuator. Arch. Mech. *70*, 391–404.

68. Kellaris, N., Gopaluni Venkata, V., Smith, G.M., Mitchell, S.K., and Keplinger, C. (2018). Peano-hasel actuators: muscle-mimetic, electrohydraulic transducers that linearly contract on activation. Sci. Robot. *3*, eaar3276.

STAR★METHODS

KEY RESOURCES TABLE

REAGENT or RESOURCE	SOURCE	IDENTIFIER
Chemicals, peptides, and recombinant proteins		
BOPP film (25 μm)	Biztem Co., Ltd., Korea	N/A
PET film (100 μm)	JONG IE NARA, Korea	N/A
Dielectric Fluid (FR3)	Cargill, USA	N/A
Carbon conductive tape	Nishin EM.CO., Ltd., Japan	N/A
Ecoflex 0030 part A	Smooth-On, Inc., USA	N/A
Ecoflex 0030 part B	Smooth-On, Inc., USA	N/A
Platinum silicone cure accelerator (productPlatcat)	Smooth-On, Inc., USA	N/A
Software and algorithms		
ProAnalyst Motion Analysis Software	Xcitex, Inc., USA	https://www.xcitex.com
Solidworks	Dassault Systems Solidworks Co., USA	https://www.solidworks.com
MATHEMATICA	Wolfram Research, Inc., USA	https://www.wolfram.com
Other		
Laser cutter (Epilog Fusion Edge - RF30w)	Epilog Laser Co, USA	N/A
Heat press (HP3805)	Xinhong Mech & Elec Co., Ltd., China	N/A
Impulse Foot Sealer (FI-450/5)	Hana Corporation Ltd., Korea	N/A
3D printer (Fortus 450mc)	Stratasys, Ltd., USA	N/A
Waveform generator (33500B series)	Keysight Technologies, USA	N/A
Power amplifier (MK-200002B)	MKPOWER, Inc., Korea	N/A
Camera (DSC-RX100M4)	Sony, Japan	N/A

RESOURCE AVAILABILITY

Lead contact

Further information and requests for resources should be directed to and will be fulfilled by the lead contact, Youngsu Cha (ys02@korea.ac.kr).

Materials availability

This study did not generate new unique reagents.

Data and code availability

All data reported in this paper will be shared by the lead contact upon request.

METHOD DETAILS

Fabrication details

To demonstrate crawling motions, we developed a new type of soft crawling robot comprising two modules, a body frame, and two pads. The head module, as an actuator, consists of a fluid-filled shell, wiring material, and flexible electrodes. The module had a trapezoidal design with a top, bottom, and height of 2.5, 5, and 5.5 cm, respectively. A 0.5 mm thick cloth was cut using a laser cutter according to the prepared design used for bone fabrication. The bone was inserted between two BOPP films. Following the prepared pattern, the two BOPP films were bonded using a heat press machine, except for the liquid injection inlet. The heating temperature was 80°C, and the heating time was 40 s. After the bone was removed, 3 mL of FR3 was injected into the shell as a dielectric fluid. Then, the fluid inlet was completely sealed using a bonding machine. All the shells were cut, leaving some margins at the edges. A carbon conductive tape was attached to both sides of the shell surface using flexible electrodes (Figure S1). The

design shape and parameters of the head module were determined as follows. The trapezoidal design was chosen for the actuator module to improve the bending action. The asymmetry of the electrode and non-electrode parts played an important role in achieving the desired bending motion.[49,64] Unlike belt-shaped soft robots, the asymmetrical design allowed forward movement by creating a structure that broke the balance at the end.[65] These results were compatible with biomimetic concepts inspired by the design of creatures with progressively decreasing widths observed in elephant trunks, and fish.[66,67] To determine the amount of liquid injected into the head module, the volume was calculated when the non-electrode section was maximally inflated. As shown in the figure, the theoretical maximum volume was obtained through a simple geometric change of the cross-section (Figure S2). The geometry was assumed to be divided into two truncated circular cylinders. When the voltage was turned off, the length of the non-electrode section was L, and the short vertical length was $2h_2$. When voltage is applied, the diameter of the base of one truncated circular cylinder was d and was obtained as follows

$$d = \frac{2L}{\pi}, \quad \text{(Equation 6)}$$

The long and short heights of the divided truncated circular cylinder were h_1 and h_2, respectively. A truncated circular cylinder was expressed as a circular cylinder with the same base area and height as $\frac{h_1+h_2}{2}$. The volumeV_c of each truncated circular cylinder was obtained as follows[68]

$$V_c = \frac{\pi d^2}{4}\frac{h_1+h_2}{2}, \quad \text{(Equation 7)}$$

$2V_c$ was set as the net volume of the pouch at maximum inflation. The parameters used in the equations are summarized in Table S1. The theoretical maximum volume was calculated to be approximately 6 mL. The dielectric fluid equivalent to 50% of the volume that can fill the non-electrode part was injected.

Next, a tail module was created to support the body. The two BOPP films were bonded according to the same design as that of the head module. 1 mL of dielectric fluid was injected into the shell and the inlet was sealed. The shell was cut along its edge with constant margins.

The body frame had a trapezoidal design that was symmetrically placed using PET films with top, bottom, and height of 3.2, 4.5, and 5 cm, respectively. Two modules were attached to the body frame.

The head pad also had a trapezoidal shape with a top, bottom, and height of 2.5, 5, and 5 cm, respectively. The PVC sheet was laser-cut according to the specified design. The head pad was attached to the bottom of the head module.

Finally, a mold was designed using the Solidworks software for tail pad manufacturing, and the design was printed using a 3D printer. The design of the mold is presented in Figure S1. The silicone solutions were mixed with Ecoflex 0030 part A, Ecoflex 0030 part B, and a platinum silicone cure accelerator in a ratio of 1:1:0.04; the resulting mixture was poured into a mold and cured at room temperature for 2 h. The tail pad was attached to the bottom end of the tail module.

Circuit configuration

The experimental setup for testing the soft crawling robot was as follows. The waveform generator and power amplifier were connected to supply power to the head module actuator of the soft robot. The input voltage was controlled using a waveform generator. The positive (+) and negative (−) ports of the power amplifier were connected to the electrodes on each side of the head module actuator. A 100 MΩ resistor was connected in parallel between the (+) and (−) ports for discharging between the electrodes. The square wave input signal used to drive the soft crawling robot included the magnitude of the input voltage and frequency. Electrohydraulic actuators typically required a pull-in voltage of more than 8 kV to operate.[45,51] Increasing the input voltage could increase the operating displacement, but could lead to electrical failure. The input peak voltage was determined to be 10 kV to ensure the long-term stable operation of the crawling robot. Also, the operation at high frequency caused the start of the next operation cycle while the robot was still stretching. Each actuation cycle had to be long enough so that the crawling robot would not enter the next cycle before fully extending. According to the continuous crawling motion results, it took about 7 s for the voltage to turn off and then start moving. This meant the time required for the electrode to discharge. Also, it took at least 12 s for the robot to unfold fully. This meant that the minimum operating

time needs 19 s for fully discharging and unfolding. The input signal was set to a frequency of 0.02 Hz and a duty cycle of 20% high signal to ensure sufficient running time for the soft crawling robot.

Recording and motion tracking

A soft crawling robot was placed horizontally on the ground to measure its movements. The movement of the crawling robot was recorded in real-time using a camera. The camera was placed on the side of the robot. The camera images were captured at 30 fps. Crawling distance data were obtained using a motion tracking program. A trace marker was attached to the end of the head module.